Elevated Photooxidation of CH$_4$ to C1 liquid products over anatase/rutile TiO$_2$ biphase junction

Hailong Tang [a], Yongqing Ma [a, b], Xiao Sun [c], Min Wang [d], Ganhong Zheng [a],

Chuhong Zhu [a],* and Meiling Wang [a],*

[a] *School of Materials Science and Engineering, Anhui University, Hefei, 230601, China*

[b] *Institute of Physical Science and Information Technology, Anhui University, Hefei 230601, China*

[c] *Hefei National Laboratory for Physical Sciences at the Microscale, Key Laboratory of Surface and Interface Chemistry and Energy Catalysis of Anhui Higher Education Institutes, School of Chemistry and Materials Science, University of Science and Technology of China, Hefei 230026, China.*

[d] *School of Physics and optoelectronics engineering, Anhui University, Hefei, 230601, China*

*To whom correspondence should be addressed.

Tel: (86) 13856996630, E-mail: mlw@ahu.edu.cn, chzhu@ahu.edu.cn

Key words: TiO$_2$, Fe-substitutional-doping, Fe$_2$O$_3$/CeO$_2$ heterojunction, photocatalysis, CH$_4$ conversion
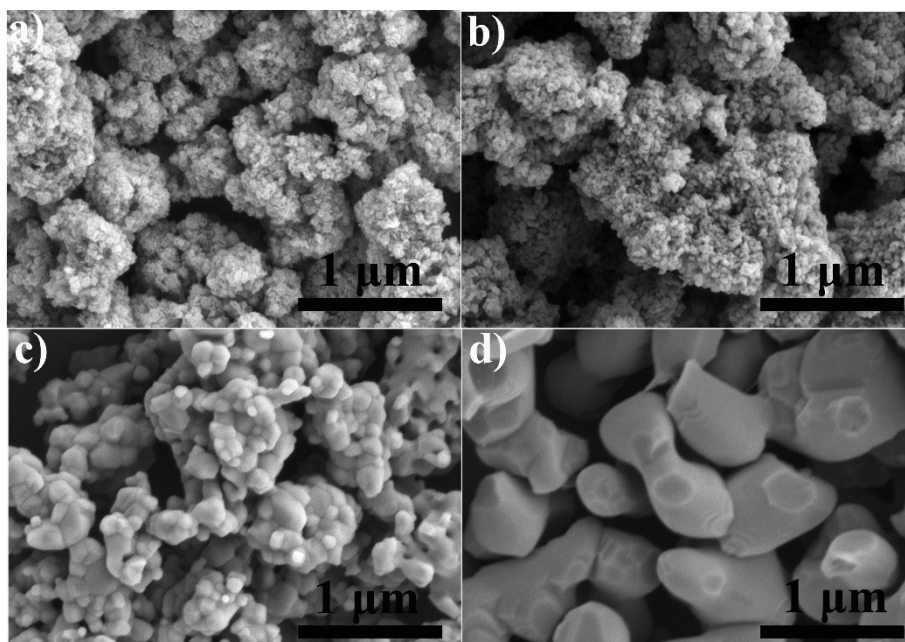
Fig. S1 SEM images of a) P25, b) P25-600/2, c) P25-800/2 and d) P25-1000/2
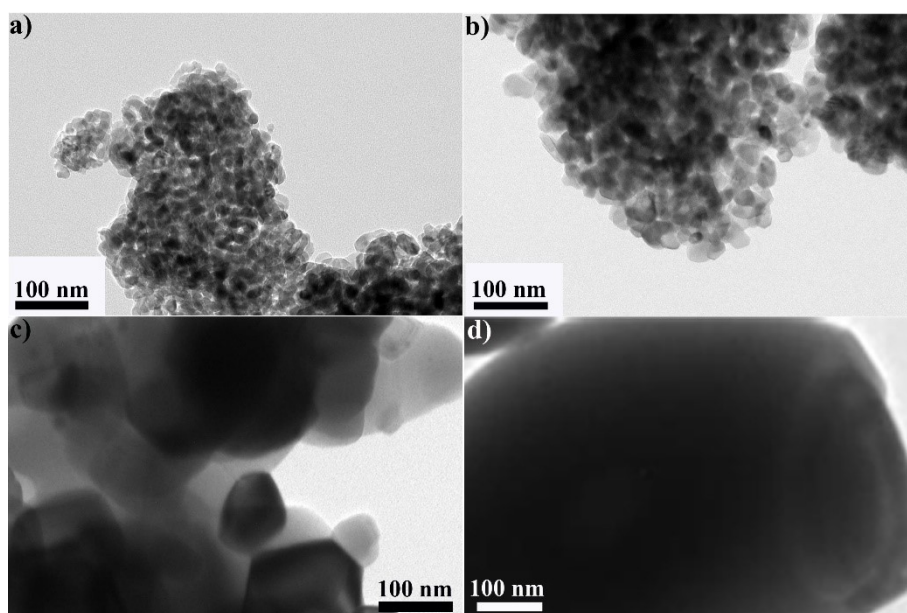
respectively.

Fig. S2 TEM images of a) P25, b) P25-600/2, c) P25-800/2 and d) P25-1000/2
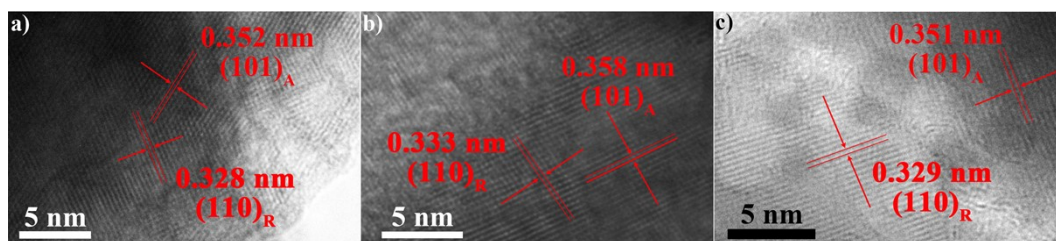
respectively.

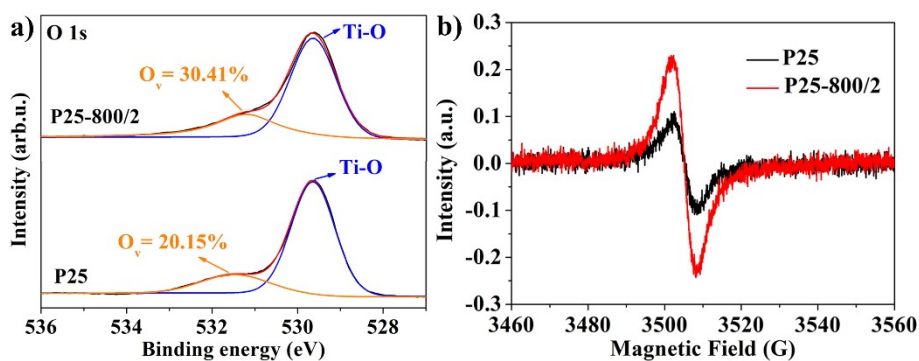Fig. S3 High resolution TEM images of the catalyst.

Fig. S4 a) Deconvoluted O 1s XPS spectra and b) ESR spectra of P25 and P25-800/2
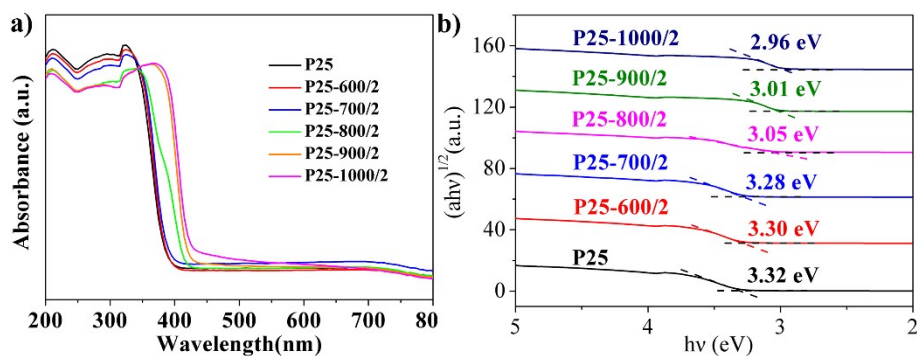
respectively.

Fig. S5 a) UV-vis diffuse reflectance spectra of varied samples, and b) their bandgaps

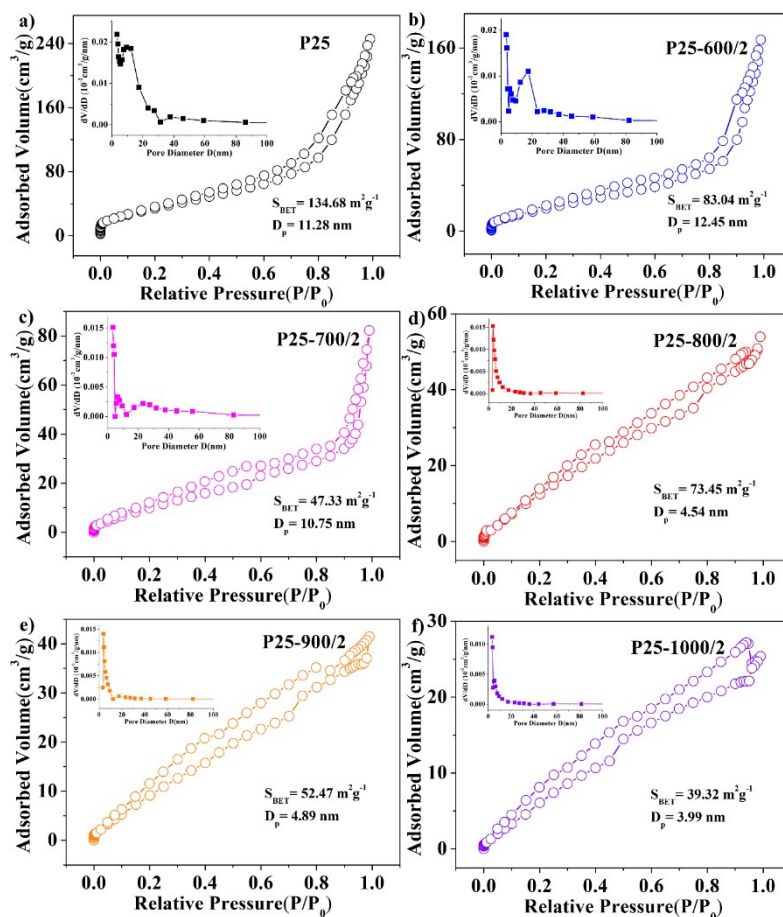determined using $[Ah\gamma]^{1/2}$ vs hγ plots.

Fig. S6 Nitrogen adsorption-desorption isotherms and their corresponding pore size distribution curves of a) P25, b) P25-600/2, c) P25-700/2, d) P25-800/2, e) p25-900/2 and f) P25-1000/2 respectively.
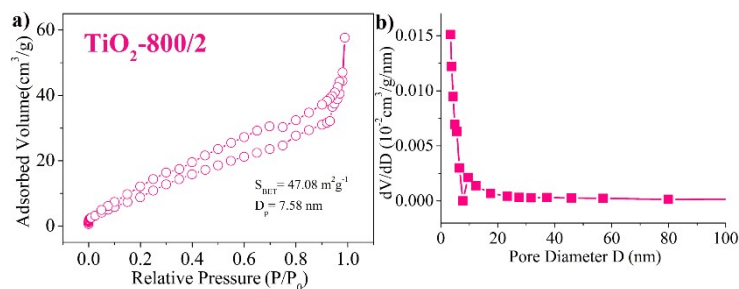

Fig. S7 a) Nitrogen adsorption-desorption isotherms and b) its corresponding pore size distribution curves of P25-800/2.

Table S1. Ratios of anatase phase and rutile phase in varied samples based on XRD patterns.

Samples	I_A	I_R	Ratio of A	Ratio of R	A/R ratio
P25-800/1	348.015	66.84	82.18%	17.82%	4.6
P25-800/2	384.265	117.01	74.42%	25.58%	2.9
P25-800/3	258.01	169.225	57.46%	42.54%	1.4

Table S2. Ratios of anatase phase and rutile phase in varied samples based on Raman spectra.

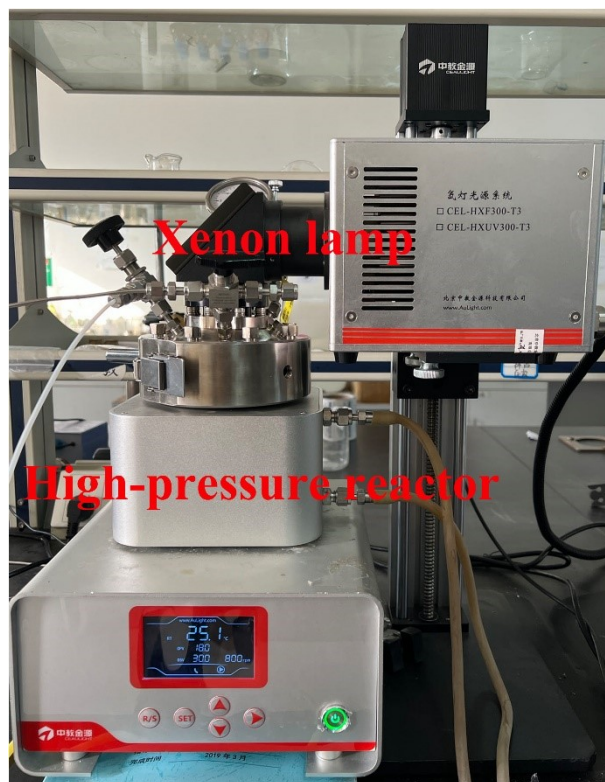| Samples	m	Ratio of A	Ratio of R	A/R ratio
P25-800/1	0.1284	83.03%	16.97%	4.9
P25-800/2	0.1868	74.91%	25.09%	3
P25-800/3	0.3289	57.04%	42.96%	1.3

Fig. S8 Photo image of the high-pressure photocatalytic reactor.
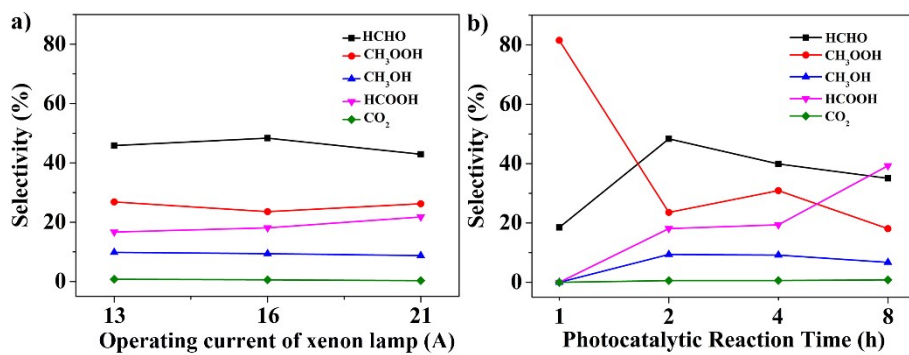

Fig. S9 Products selectivity as a function of a) operating current of xenon lamp and b)
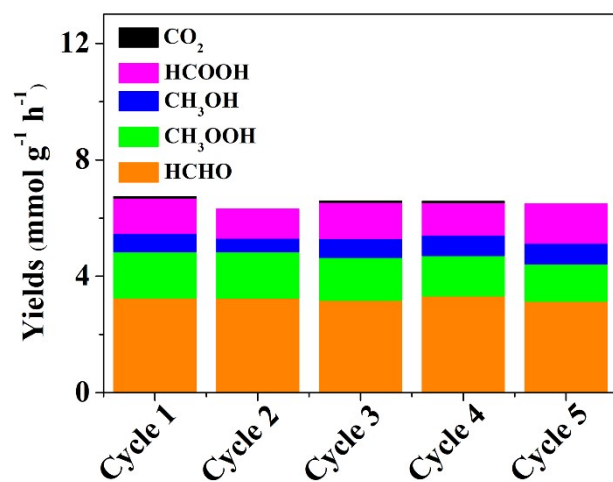
illumination time.

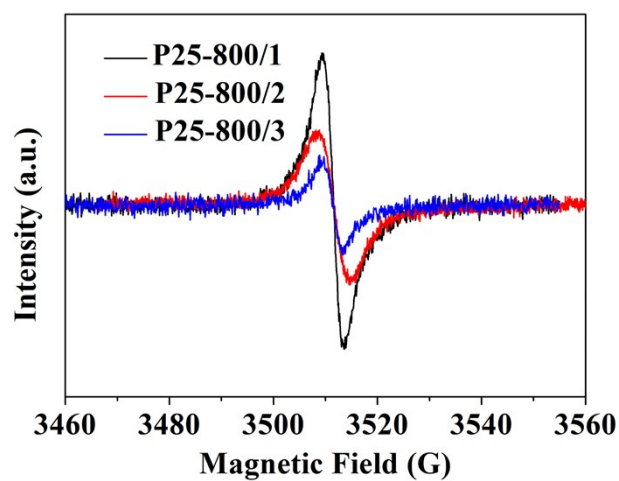Fig. S10 Histograms of products yields during cycling tests.

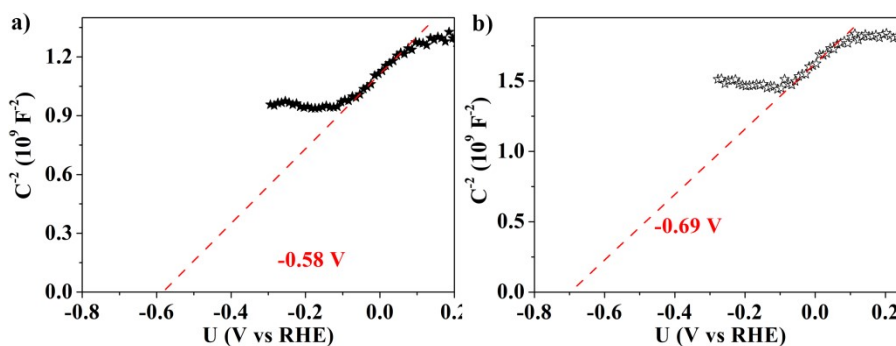Fig. S11 ESR spectra of P25-800/1, P25-800/2 and P25-800/3 respectively.

Fig. S12 Mott−Schottky plots of a) A-TiO$_2$ and b) R-TiO$_2$ at frequency of 1 kHz.
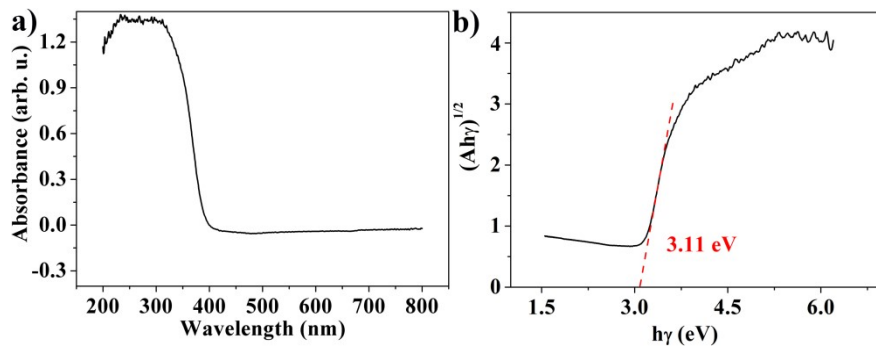
Fig. S13 a) UV-vis DRS spectrum of A-TiO$_2$ and b) its bandgaps determined using

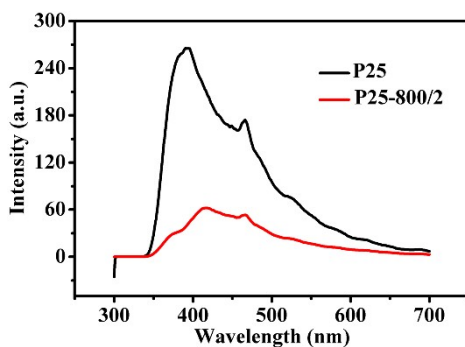the [Ahγ]$^{1/2}$ vs hγ plot.

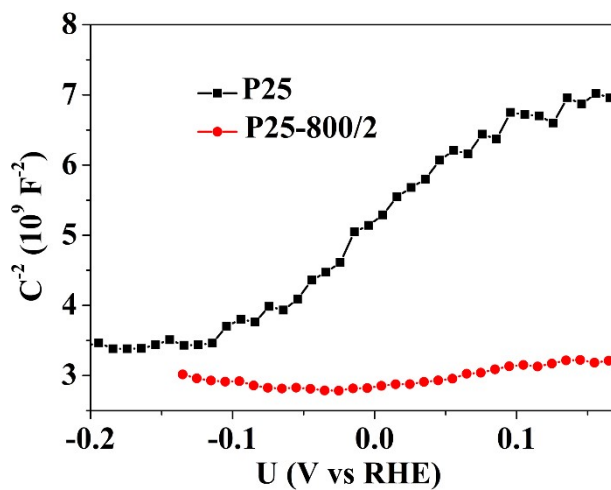Fig. S14 PL spectra of P25 and P25-800/2.

Fig. S15 Mott−Schottky plots of P25 and P25-800/2.
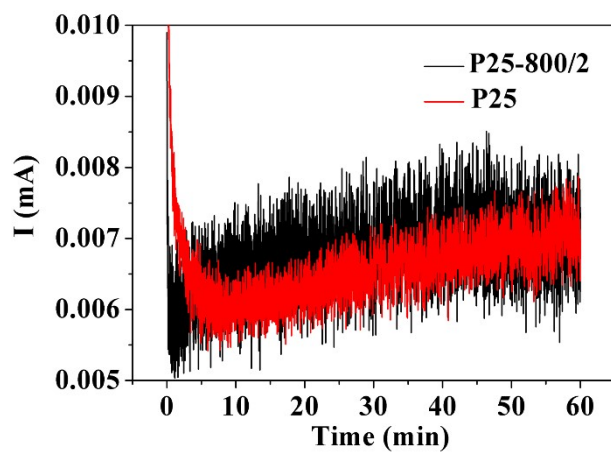
Fig. S16 Photocurrent curves of P25 and P25-800/2.

Fig. S17 EIS spectra of P25 and P25-800/2.
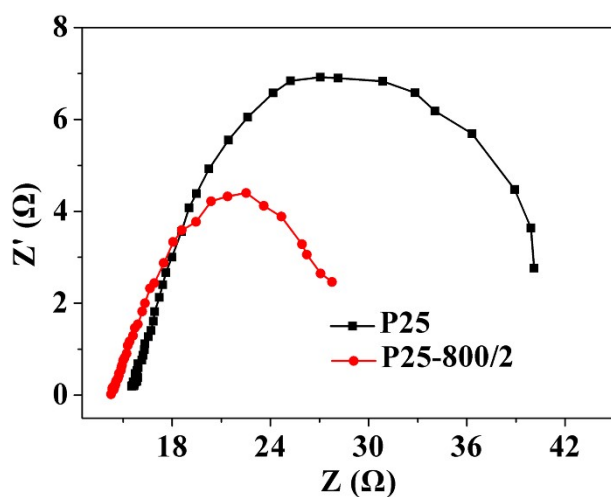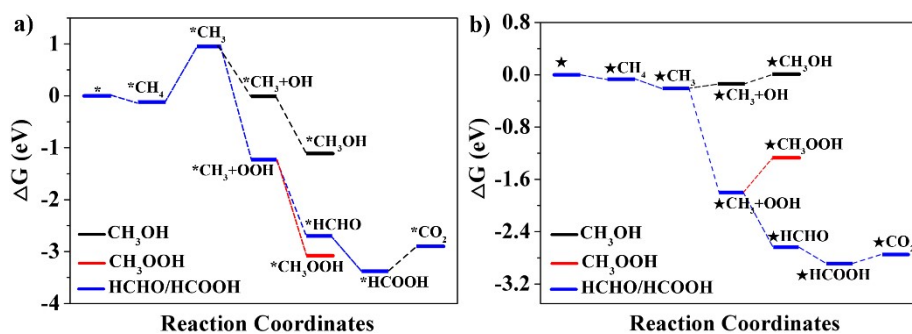

Fig. S18 Probable reaction routes and DFT energy profiles for the formation of varied

C1 products on a) A-TiO$_2$ (101) and b) R-TiO$_2$ (110) planes.
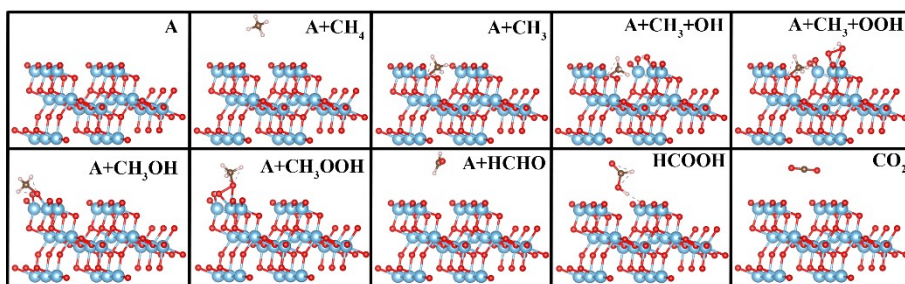
Fig. S19 Structures of the main intermediates during CH_4 conversion to varied products on A-TiO_2 (101) plane.
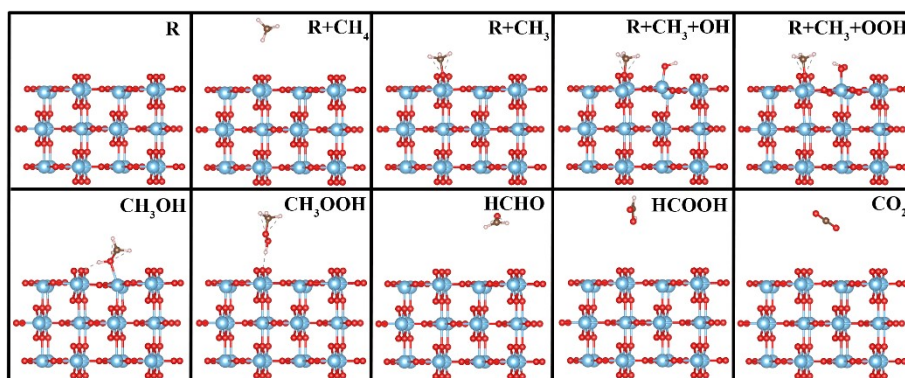
Fig. S20 Structures of the main intermediates during CH_4 conversion to varied products on R-TiO_2 (110) plane.

Fig. S21 Calculated PDOS of a) A-TiO$_2$ (101), b) R-TiO$_2$ and c) A/R heterostructure

respectively.

Table S3 Desorption energy of varied products.

Products	CH$_3$OH	CH$_3$OOH	HCHO	HCOOH
Desorption energy (eV)	1.235	0.624	0.2149	0.228
Adsorption configurations				

Part S1 Details of the instruments used for catalyst characterization

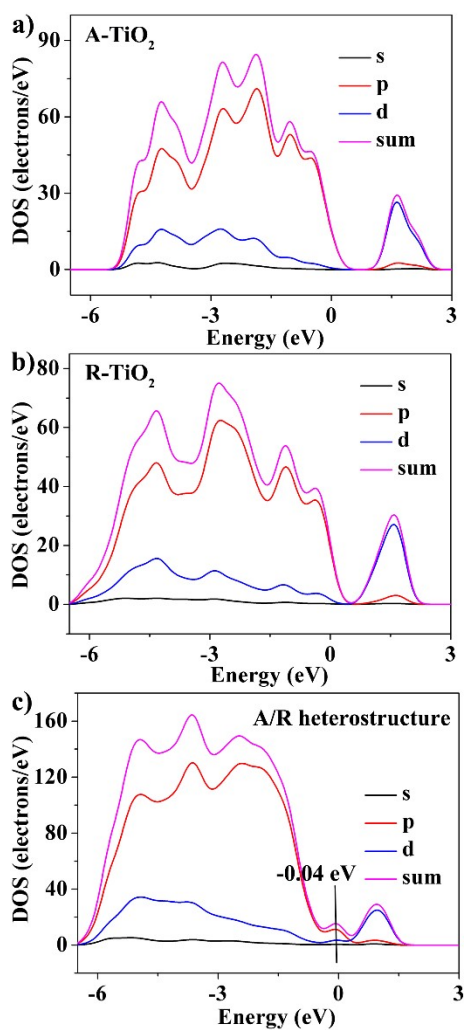Morphologies and lattice fringe images of varied catalysts were measured on the S-4800 scanning electron microscopy (SEM, Hitachi, Japan) and JEOL JEM-2100 transmission electron microscopy (TEM, Japan). Crystal structures were characterized by a X-Ray Diffractometer (Japan). UV–vis diffuse reflectance spectra were obtained on a U-4100 UV-vis absorption spectrometer (Japan). Surface elemental chemical states were characterized by a ESCALAB 250Xi X ray photoelectron spectrometer (USA). Specific surface areas/pore sizes were measured on a Quantachrome autosorb-iQ automatic specific surface and porosity analyzer (USA). All H nuclear magnetic resonance (HNMR) spectra were recorded on a JNM-ECZ400S NMR spectrometer (Japan). Electron spinning resonance (EPR) spectra were measured on a ESR spectrometer (EMX plus 10/12, Bruker, Germany). In-situ Fourier transform infrared (FTIR) spectra were recorded on the Vertex 80/Hyperion 2000 spectrometer (Bruker, Germany).

Part S2 DFT computational details.

All the density functional theory (DFT) calculations were carried out using the Dmol[3] code of Materials Studio 2019.[1] The exchange-correlation potential was calculated by the generalized gradient approximation (GGA) with the Perdew-Burke-Ernzerhof

(PBE) functional.[2] The interactions between electronics and ions were described using the DFT semi-core pseudo potentials (DSPPs) core treatment, which replaces core electrons by a single effective potential and introduces some degree of relativistic correction into the core.[3] The geometry optimization convergences tolerance was set to 5×10^{-4} Ha·Å^{-1} (1 Ha = 27.21 eV), and the total energy convergences was set to 10^{-6} Ha. The Brillouin zone were sampled with $1\times1\times1$, $2\times1\times1$ and $1\times1\times1$ Monkhorst-Pack k-point meshes for A-TiO$_2$ (101), R-TiO$_2$ (110) and A/R heterostructure model respectively, and a smearing of 0.005 Ha was applied to speed up electronic convergence. The Ti and O atoms in the bottom two layers were fixed, and the others atoms were fully relaxed. The thickness of the vacuum layer was set as 20 Å to avoid the unwanted interaction between the slab and its period images.

1 B. Delley. From molecules to solids with the DMol3 approach, The Journal of Chemical Physics., 2000, 113, 7756-7764.

2 J. P. Perdew, K. Burke, M. Ernzerhof, Generalized gradient approximation made simple, Phys. Rev. Lett., 1996, 77, 3865.

3 B. Delley, Hardness conserving semilocal pseudopotentials, Phys. Rev. B., 2002, 66, 155125.